Silicon-Organic Hybrid Electro-Optical Devices

Juerg Leuthold, *Fellow, IEEE*, Christian Koos, Wolfgang Freude, *Senior Member, IEEE*, Luca Alloatti, Robert Palmer, Dietmar Korn, Joerg Pfeifle Matthias Lauermann, Raluca Dinu, Silvan Wehrli, *Student Member, IEEE*, Mojca Jazbinsek, Peter Günter, Michael Waldow, Thorsten Wahlbrink, Jens Bolten, Heinrich Kurz, Maryse Fournier, Jean-Marc Fedeli, Hui Yu, and Wim Bogaerts, *Member, IEEE*

(Invited Paper)

***Abstract*—Organic materials combined with strongly guiding silicon waveguides open the route to highly efficient electro-optical devices. Modulators based on the so-called silicon-organic hybrid (SOH) platform have only recently shown frequency responses up to 100 GHz, high-speed operation beyond 112 Gbit/s with fJ/bit power consumption. In this paper, we review the SOH platform and discuss important devices such as Mach–Zehnder and IQ-modulators based on the linear electro-optic effect. We further show liquid-crystal phase-shifters with a voltage-length product as low as $V_\pi L = 0.06$ V·mm and sub-μW power consumption as required for slow optical switching or tuning optical filters and devices.**

***Index Terms*—Integrated optics, silicon, organic materials, liquid crystals, nanophotonics, elecrooptic modulators.**

I. Introduction

SILICON photonics when combined with the many options offered by organic molecules forms the base of a powerful technology - the *silicon-organic hybrid* (SOH) platform [1], [2]. This platform is of considerable interest since it adds strong linear-electro-optic effect and a variety of other optical properties to the toolbox of silicon photonics.

A platform that allows for a smooth cointegration of passive and active photonic devices, and that also has the potential to cointegrate photonics with electronics, is one of the long-term visions of the datacom and telecom industry. There are only a few platforms that could meet the combined needs of the photonics and electronics world. The few contenders are the Si, the InP, and the GaAs semiconductor platforms. Among these, the silicon platform is unique because the material is widely available at low cost and is already the mainstay of the electronics industry [3]. However, silicon has issues when applied for photonics. Due to its centro-symmetric crystal structure it does not provide a $\chi^{(2)}-$ nonlinearity, and thus defie building of electro-optic modulators based on the linear-electro-optic effect. On the other hand, the $\chi^{(3)}-$ nonlinearity is sufficientl large but its usefulness is diminished by two-photon absorption (TPA). Finally, crystalline silicon does not support spontaneous emission of light, so an integrated silicon laser remains an elusive challenge of its own right.

While the silicon photonics community has responded to these challenges with a set of innovative monolithically integrated solutions [4], there have been numerous activities with respect to the SOH platform that increasingly holds promise to overcome most obstacles [2]. In the SOH approach, optical modes are strongly guided by conventional silicon-on-insulator (SOI) waveguides, but the functional properties of the waveguide have their origin in an organic nonlinear cladding. Thanks to the large variety of organic cladding materials, almost any property can be grafted onto a waveguide [5]–[12].

In this paper, we firs review the SOH approach in general. We then focus on the SOH Pockels effect phase-shifter. Due to the fast response, it is ideal for use in modulators. We then discuss different modulator realizations, such as the Mach–Zehnder (MZ) modulators or the in-phase/quadrature-phase (IQ) modulators. Bandwidth, power consumption, and drive voltage are considered in detail. Finally, we report on an alternative approach which exploits a liquid–crystal cladding instead of a $\chi^{(2)}-$ cladding for building phase-shifters. The result is a phase-shifter with record high efficien y and record low-power consumption but a slow response. These phase-shifters are ideal for tuning filte responses.

II. SOH—The Platform

In the SOH approach, a conventional SOI waveguide is functionalized with an organic cladding material. This way critical

Manuscript received April 4, 2013; revised June 25, 2013; accepted June 26, 2013. This work was supported in part by the EU-FP7 Project SOFI under Grant 248609, in part by the BMBF joint project MISTRAL, in part by the DFG Center for Functional Nanostructures, in part by the Helmholtz International Research School on Teratronics (HIRST), in part by the Karlsruhe School of Optics and Photonics (KSOP), and in part by the Karlsruhe Nano-Micro Facility. This work was further supported by the European Research Council (ERC Starting Grant 'EnTeraPIC', number 280145) and ePIXfab.

J. Leuthold and P. Günter are with the ETH-Zurich, 8092 Zurich, Switzerland (e-mail: JuergLeuthold@ethz.ch; gunter@rainbowphotonics.com).

C. Koos, W. Freude, L. Alloatti, R. Palmer, D. Korn, J. Pfeifle and M. Lauermann are with the Karlsruhe Institute of Technology, Karlsruhe 76133, Germany (e-mail: Christian.Koos@kit.edu; W.Freude@kit.edu; luca.alloatti@kit.edu; robert.palmer@kit.edu; Dietmar.Korn@kit.edu; Joerg.Pfeifle@kit.edu matthias.lauermann@kit.edu).

R. Dinu and S. Wehrli are with the GigOptix, Inc., Zürich CH-8008, Switzerland (e-mail: rdinu@gigoptix.com; swehrli@gigoptix.com).

M. Jazbinsek and P. Günter are with the Rainbow Photonics AG, Zurich 8048, Switzerland (e-mail: mojca@rainbowphotonics.com).

M. Waldow, T. Wahlbrink, and H. Kurz are with the AMO GmbH, Aachen 52074, Germany (e-mail: waldow@amo.de; wahlbrink@amo.de; kurz@amo.de).

J. Bolten and J. M. Fedeli are with the CEA, LETI, Minatec 17 rue des Martyrs, 38054 Grenoble, France (e-mail: bolten@amo.de; jean-marc.fedeli@cea.fr).

M. Fournier is with the Department of Optronics, CEA Grenoble Grenoble 38054, France (e-mail: maryse.fournier@cea.fr).

H. Yu is with the Photonics Research Group, Department of Information Technology, Ghent University – IMEC, Gent 9000, Belgium (e-mail: afterglow.yuhui@gmail.com).

W. Bogaerts is with the Photonics Research Group, Department of Information Technology, Ghent University – IMEC, Gent, Belgium (e-mail: wim.bogaerts@intec.ugent.be).

Color versions of one or more of the f gures in this paper are available online at http://ieeexplore.ieee.org.

Digital Object Identifie 10.1109/JSTQE.2013.2271846

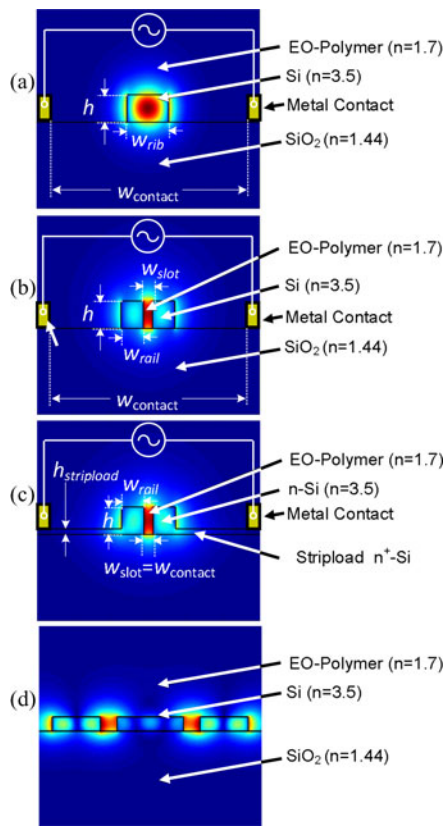

Fig. 1. Different types of silicon organic-hybrid waveguides with magnitude of electric fiel plotted for quasi-TE modes. (a) Strip waveguide with an organic cladding. (b) Slot waveguide where the light is strongly confine to the slot fille with an organic material. (c) Strip-loaded slot waveguide where metal electrodes are connected to the two rails of the slot waveguide by doped silicon strips (stripload). Both, the modulating fiel and the optical mode are well confine to the slot. For efficien electro-optic modulation the slot needs to be fille with an adequate electro-optic material. Plots derived from [28]. (d) High-order mode for double-slot waveguide dispersion-engineered for phase-matched difference-frequency generation (DFG) [17].

fabrication steps can rely on high-yield processes based on CMOS fabrication technology of an SOI wafer and the functional organic material can subsequently be deposited onto the wafer. Typical organic cladding materials vary from highly nonlinear $\chi^{(3)}$ oligomers such as DDMEBT [13] for efficien four-wave mixing [8], to highly-nonlinear $\chi^{(2)}$ chromophores [14], [15] for high-speed modulation [16] and difference-frequency generation [17], to polymer-dispersed dyes for optically pumped lasers [18], [19], to liquid-crystals for low-voltage phase-shifters [20].

In the following, we discuss two important components: Active SOH waveguides, and the strip-to-slot converter that is needed to perform a transition from passive strip to active slot waveguides.

A. SOH Waveguide Structures

For maximizing the optical interaction with the organic cladding and for optimizing other device-dependent properties such as minimizing TPA, maximizing the overlap with an external modulating field optimizing phase-matching between different optical modes, or minimizing optical losses, the designer can choose between four basic waveguide structures: A simple strip waveguide, a slot waveguide, a strip-loaded slot waveguide, and a double-slot waveguide; see Fig. 1. The properties of these waveguides are summarized in Table I. All waveguides depicted in Fig. 1 share the common feature of having a high-refractive index core (n_{Si}=3.48) and a low-refractive index organic cladding (which typically ranges between 1.5 and 2). When considering quasi-TE modes, the discontinuity of the refractive index leads to a discontinuity of the electric field an effect which is known as "field-enhancement [2] and improves the optical interaction between the optical mode and the cladding. Additionally, the SOH concept allows the user to freely choose the cladding among the immense variety of available organic molecules, many of which have been developed and optimized for longer than a decade [13]–[15].

In the following, we review these waveguide structures with respect to their ability for nonlinear applications and electro-optic modulation.

1) *Strip waveguide, see* Fig. 1(a): The advantage of the strip waveguide is ease of fabrication and low optical losses. In strip waveguides, losses are meanwhile approaching 0.2 dB/mm [21]. (Remark: In ridge waveguides with lower mode confinemen losses are below 0.2 dB/mm [22] and in planar waveguides with very weak guiding even record low losses of 0.1 dB/m have been reported [23]). Phase-shifters with polymer cladding [24] and with liquid crystals [25] have been demonstrated with strip waveguides, but the large separation of the contact electrodes used for modulation, which is typically a few microns require relatively high driving voltages.
2) *Slot waveguide, see* Fig. 1(b): The structure offers a high confinemen of the optical mode in the slot [5], [8]. This has been successfully exploited for reducing TPA in the silicon core for nonlinear processes at high optical powers [8], [26] and for increasing the optical interaction with optical dies for lasing [18]. The slot is however more difficul to fabricate and often requires high-resolution 193 nm DUV lithography or e-beam lithography. The fiel enhancement on the slot sidewalls also increases propagation losses, which are typically in the range 0.7–1.5 dB/mm [21], but are expected to decrease as advanced technologies improve the surface smoothness [27]. And while vertical slots so far are more common [5], [28], [29], ease of fabrication might also make a good case for horizontal slots [30].
3) *Strip-loaded slot waveguide, see* Fig. 1(c): This structure is ideal for electro-optic devices [9]–[11]. Its conductive silicon strip-loads connect the two rails of the slot waveguide with metal electrodes [2], [11]. If the strip-load resistance is sufficientl low, a voltage applied on the metal electrodes will almost entirely drop across the slot. The ribs to both sides of the slot and the slot itself can be optimized so that quite a fraction of the optical signal is in the cladding [17].
   Since the slot is typically only 100 nm wide, and both electrical and optical modes almost ideally overlap in the narrow slot, only low voltages are needed to induce a very high refractive index change in the nonlinear material of

TABLE I
CHARACTERISTICS OF SILICON-ORGANIC HYBRID WAVEGUIDE STRUCTURES

Characteristics of SOH Waveguide	Strip, Fig. 1(a)	Slot, Fig. 1(b)	Strip-Loaded Slot, Fig. 1(c)	Double-Slot Fig. 1(d)
Typical applications	FWM, modulation	FWM, modulation, optical pumped lasing	High-speed and low-voltage modulation	DFG, SHG
Typical claddings	$\chi^{(3)}$ [26], $\chi^{(2)}$ [24], Liquid crystals [25]	$\chi^{(3)}$ [8], Optical dies [18]	$\chi^{(2)}$ [16], Liquid crystals [20]	$\chi^{(2)}$ [17]
Fabrication Complexity	Simple: low lithography resolution, single etch step	Medium: Requires high resolution for slot definition	High: Requires strip-load and high-res. lithography. Requires doping and metallization	Simple: single etch step. Large slot size: no high resolution lithography needed
Confinement of optical field in nonlinear cladding, exemplary values	Moderate [29] Field in cladding e.g. 0.33[1]	High [29], [30] Field in all cladding e.g. 0.82 and in slot 0.30[2]	High [11] Field in all caldding e.g. 0.62 and in slot 0.23[3]	High [17]
Optical losses	Low [21]	Moderate [21]	High with doping, Moderate with accumulation layers [31]	Possibly Low
Voltage-length product VπL (for modulation only)	High	Moderate	Low	
Dominant Bandwidth limitation (for modulation only)	RF losses, Walk-off	RF losses, Walk-off	RC time constant	
Power consumption (for modulation only)	Low	Low	Ultra-low	
Radio-frequency (RF) attenuation of travelling-wave electrodes [32]	≈0.5 dB/cm @ 100GHz	≈0.5 dB/cm @ 100GHz	≈5 – 10 dB/mm @ 100GHz	

[1]Exemplarily we choose $w_{\mathrm{rib}} = 350$ nm, $h = 220$ nm, $\lambda = 1.55$ µm and $n_{\mathrm{Si}} = 3.48$, $n_{\mathrm{SiO2}} = 1.44$, and $n_{\mathrm{Polymer}} = 1.7$.
[2]Exemplarily we choose $w_{\mathrm{rail}} = 175$ nm, $w_{\mathrm{slot}} = 120$ nm, $h = 220$ nm, $\lambda = 1.55$ µm and $n_{\mathrm{Si}} = 3.48$, $n_{\mathrm{SiO2}} = 1.44$, and $n_{\mathrm{Polymer}} = 1.7$.
[3]Exemplarily we choose $w_{\mathrm{rail}} = 175$ nm, $w_{\mathrm{slot}} = 80$ nm, $h = 220$ nm, $h_{\mathrm{stripload}} = 50$ nm, $\lambda = 1.55$ µm and $n_{\mathrm{Si}} = 3.48$, $n_{\mathrm{SiO2}} = 1.44$, and $n_{\mathrm{Polymer}} = 1.7$.

the slot. The structure has to be engineered for low optical and low RF electrical losses though. Optical losses are not only due to imperfect surfaces but also due to free-carrier absorption (FCA) from the doped strip loads. For making the silicon strips sufficientl conductive without causing excessive optical losses, it has been suggested to use gate-induced accumulation layers instead of ion-implantation [31]. Further, the structure has to be optimized for low RF losses which again are in part due to the conductive strip loads [32]. The fabrication of this type of waveguide is the most elaborate, and requires high-resolution lithography, different etch depths, ion implantation, metallization, and passivation [16].

4) *Double-slot waveguide, see* Fig. 1(d): This type of waveguide can be dispersion-engineered to achieve phase-matching using higher order quasi-TE modes for second-order nonlinear optical mixing such as mid-IR difference and sum-frequency generation (DFG, SFG) as well as second harmonic generation [17]. Most of the light is confine inside the slots, and this fiel concentration again maximizes the nonlinear optical interaction with the $\chi^{(2)}$.

The various advantages and disadvantages of the four structures are summarized in Table I. A more extensive review on nonlinear effects in silicon may be found in [33].

In the following, we will concentrate on Fig. 1(c) since this is the preferred geometry for building the most efficien electro-optic SOH modulators.

B. Strip-to-Slot Converter

The standard waveguides in silicon photonics are strip waveguides. If a silicon circuit comprises active sections with slot waveguides, then these typically must be accessed via strip waveguides, meaning that strip-to-slot converters are needed. These converters must meet the following objectives.

1) The transition must occur with low losses as well as low reflection for avoiding multipath interference.
2) The two rails definin the slot must remain electrically separated, since these are connected to electrodes with different potentials [16].

Previously proposed strip-to-slot converters were based on linear tapers [34]. A Y-shaped converter has been proposed by Brosi *et al.* [11] and a transition loss of 0.13 dB has been reported [35]. Recently, a very short strip-to-striploaded slot waveguide converter has been introduced that meets all the above listed requirements with losses of 0.02 dB per converter [28]. We summarize the results of this publication and refer the reader to [28] for more details.

Fig. 2(a) depicts the low-loss converter for coupling a strip waveguide to a strip-loaded slot waveguide. The converter comprises two sections. In each of the sections, the width of one of the two rails of the slot waveguide is logarithmically tapered. Further, the two rails of the slot waveguide are attached to 45-nm-thick silicon striploads that connect the waveguide to metal electrodes. The stripload is tapered at the begin of Section I to ensure a smooth transition.

The strip-to-slot converters as depicted in Fig. 2(a) were realized with the following parameters. In converter Section I, the slot width w_{slot} has been tapered down logarithmically from 240 to 120 nm, and rail 2 tapers up from 120 to 240 nm. Section II comprises the logarithmic taper of rail 1 to the fina symmetric strip-loaded slot waveguide. The slot width and the width of rail 2 remain constant in this section. The lengths of Sections I and II were 4 μm and 8 μm, respectively. The strip was 240 nm thick, and the stripload section was as thin as 45 nm.

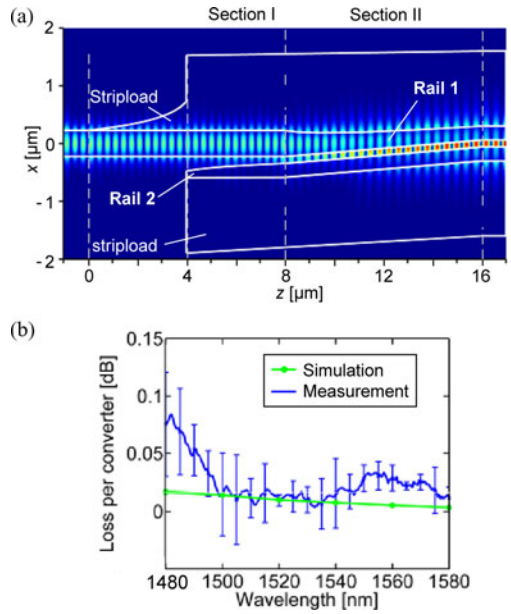

Fig. 2. (a) Simulation showing how a signal in a strip waveguide is mapped into a slot waveguide by means of a strip-to-stripload converter. The plot shows the electric fiel distribution in the logarithmically tapered strip-to-striploaded slot mode converter. To the left of Section I one can also see a one-sided logarithmic uptaper of the stripload. (b) Measured loss per converter in a wavelength range between 1480 and 1580 nm. The average loss in this wavelength range is 0.02 dB per converter [28].

Results of the experimentally realized tapers from e-beam lithography in a wavelength range from 1480 to 1580 nm are shown in Fig. 2(b). The average loss per converter is as low as 0.02 dB in the measured wavelength range. The losses are plotted as loss per converter, while the actual experimental results are derived from a cascade of 30 pairs of strip-to-slot and slot-to-strip converters.

III. SOH Modulators

Modulators are key elements in optical communications. They are needed to encode information onto an optical carrier. In the past, information was mostly encoded by on-off keying onto an optical carrier and turning the light ON and OFF with suffi cient extinction ratio was considered good enough. Meanwhile, information is often encoded using the quadrature-amplitude modulation (QAM) format, a modulation format where multiple levels of both phase and amplitude are encoded [36], [37]. In the foreseeable future software define transmitters will be used to encode any shape (including precompensation) and any modulation format onto an optical carrier [38]. Future modulators thus need to reliably encode any point on the complex constellation space on an optical carrier. In the industry such amplitude and phase-encoding is typically realized with MZ and IQ modulators. Both MZ- and IQ-modulators need true phase-shifters as basic building blocks. Subsequently, we discuss the MZ- and IQ-modulator configuration and comment on possible implementations paths.

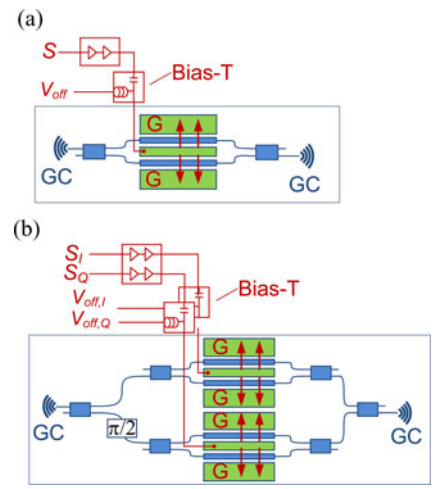

Fig. 3. Modulator configuration (a) Mach–Zehnder (MZ) modulator. An electrical data signal (S) drives the MZ-modulator by means of CPW GSG-electrodes. The GSG electrodes are arranged such that oppositely directed electric slot field (red arrows) build up across the waveguides so that the MZ is operated in push–pull mode. (b) IQ-modulator configuratio where an in-phase (S_I) and a quadrature phase data signal (S_Q) drive a nested MZI configuration This configuratio allows encoding of any amplitude and phase relation onto the signal envelope. The abreviations (GC) stand for grating couplers, $V_{\rm off}$ is a dc offset voltage used to adjust the phase relation of the interferometer.

A. MZ and IQ Modulator Configu ation

We begin the discussion by introducing the transfer function of a MZ modulator with phase-shifters on its arms

$$E_s = \frac{1}{2} e^{j\left(\frac{\vartheta_1+\vartheta_2}{2}\right)} \cos\left(\frac{\vartheta_1-\vartheta_2}{2}\right) \tag{1}$$

where ϑ_1 and ϑ_2 are the phase changes when applying a voltage to the phase modulators (PM) in the respective upper and lower arms of the MZ. It can be seen that an ideal chirp-free amplitude-shift keying signal is obtained for operating the device in "push–pull" mode—i.e., when the phases induced in the upper and lower arms of the MZ interferometer are chosen to have opposite signs, $\vartheta_2 = -\vartheta_1$. As an advantage of the "push–pull" operating mode, ON-OFF switching only requires switching the phases in the arms between $+\pi/2$ and $-\pi/2$, so that full switching requires a voltage swing of $V_\pi/2$ only rather than V_π, with V_π the voltage required to shift the phase by π. An MZ modulator configuratio is depicted in Fig. 3(a).

By nesting two MZ modulators where each is operated in push–pull mode and both are offset by $\pi/2$, one can encode the in-phase and quadrature information of a signal independently. Often a bias-T is used to adjust the relative phase within the interferometer by a dc offset voltage $V_{\rm off}$. The MZ and IQ modulator configuration are depicted in Fig. 3.

B. SOH "Push–Pull" Phase Modulator

Phase-modulators are not straight forward to implement in silicon, as the material is centro-symmetric and does not offer a linear-electro-optic effect. Yet, the silicon photonics community has found ways to build modulators using the plasma effect [4]. This means that free carriers are either injected [39] or extracted [40] from a p-n/p-i-n-junction or capacitor located

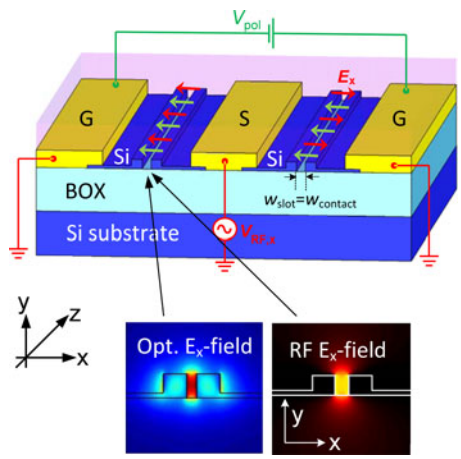

Fig. 4. Schematic cross section of an SOH Mach–Zehnder (MZ) modulator, showing two phase modulators with Si strip-loaded slot waveguides (WG), fille and covered with a nonlinear cladding. Coplanar RF transmission lines (GSG, ground-signal-ground) are arranged along the slot waveguides. If an RF voltage is applied on the S-electrode it creates oppositely directed electric field in the slot (red arrows). If the nonlinear material is poled along one direction (green arrows) the modulating RF voltage leads to opposite phase shifts in both interferometer arms. The lower left inset depicts the color-coded dominant x-component $|E_x|$ of the optical electric fiel in the slot WG cross section. The lower right inset displays the modulating electrical RF field Both field are strongly confine to the slot. The Figure is derived from [47].

within the silicon waveguide. This way the permittivity changes due to a free-carrier refractive index (FCI) variation. However, FCI is inevitably accompanied by FCA [41]. This makes accessing a particular point within a complex constellation diagram more difficult Despite these obstacles, plasma effect silicon modulators for QPSK signals [42], 16QAM signals [43] and with bandwidths of up to 50 GHz have been demonstrated [44]. Alternatively, some groups have been growing strained silicon layers, thereby breaking the centro-symmetry of crystalline silicon such that a linear electro-optic effect could be exploited [45], [46].

The SOH platform allows for an alternative path toward the realization of a true phase-modulator [9]–[11], [16]. To explain the operation principle in more detail, we show a sketch through the cross section of an MZ modulator in Fig. 4. This figur shows the upper and lower arm of the strip-loaded slot waveguides that form the MZ-modulator of Fig. 3(a) together with the ground-signal-ground (GSG) travelling wave RF electrodes. The two slot waveguides shown in blue are fille with the nonlinear electro-optic material. A simulation of the optical fiel in the slot is shown in the lower left inset. It can be seen that the large index contrast between Si of $n_{\mathrm{Si}} = 3.48$ and the nonlinear polymer $n_{\mathrm{poly}} = 1.7$ causes an enhancement of the dominant electrical fiel of the optical quasi-TE wave inside the slot. The ribs of the slot are connected to the GSG electrodes of a coplanar RF waveguide. When an RF voltage is applied to the metals and by this to the conductive striploads of the Si rails, the electric fiel drops off across the slot fille with the nonlinear, insulating polymer (lower right inset). This way the optical and electrical field are both confine to the narrow slot such that the overlap of the two field is high resulting in an efficien modulation.

We now become more quantitative and state the total phase shift obtainable with an electro-optic modulator of length L [11]

$$\Delta\phi_0 = k_0 \Gamma \, \Delta n \, L \tag{2}$$

where k_0 is the wave number of the signal and the refractive index change Δn is proportional to the electro-optic coefficien r_{xxx}

$$\Delta n = -\frac{1}{2} n_x \, r_{xxx} \, E_{\mathrm{RF},x} \, , \qquad E_{\mathrm{RF},x} = V_{\mathrm{RF},x} / w_{\mathrm{Contact}} \tag{3}$$

where the RF electric fiel $E_{\mathrm{RF},x}$ is aligned along the x-axis and is due to a voltage $V_{\mathrm{RF},x}$ applied across the slot of width w_{Contact} and where the optical transverse electric fiel E_x is propagating in an electro-optic material with refractive index n_x along the x-axis. We further have the interaction factor Γ:

$$\Gamma = \int_{\mathrm{gap}} \frac{n_x}{Z_0} \, |E_x|^2 \, dA \Big/ \int \Re \left(\vec{E} \times \vec{H}^* \right) \cdot \vec{e}_z \, dA \tag{4}$$

with Z_0 the free-space wave impedance, $\vec{E}$ and $\vec{H}$ the electrial and magnetic field of the optical mode, and $\vec{e}_z$ the unit vector along the propagation direction. It should be stressed that Γ is not the confinemen factor, which usually gives the ratio of the total power in the active section to the total power of the mode. Here, Γ is only the ratio of the power that interacts with the material and the applied electrical fiel to the total power. So for instance, in our case only the components $|E_x|^2$ transverse to the slot and in parallel to the applied electrical fiel $E_{\mathrm{RF},x}$ contribute to the interaction [11].

As an example, we calculate the interaction factor of the strip loaded-slot waveguide from Fig. 1(c) with the waveguide dimension as per footnote of Table I. The total interaction of the optical fiel with the nonlinear cladding is $\Gamma = 0.62$. Yet, only a fraction of $\Gamma = 0.23$ of the signal is in the slot where the electrical fiel is strongest. A fraction of 0.39 of the light is in the cladding and will contribute only little to the refractive index change; thus, one could conclude that the structures from Fig. 1(a) or (b) might be more advantageous. Yet, what really matters is the total phase-shift for a given applied voltage $V_{\mathrm{RF},x}$. This total phase-shift increases to the same extent as w_{Contact} decreases. In the strip and slot structures of Fig. 1(a) and (b), the metallic contact w_{Contact} would typically be 3.2 μm apart from each other. In the strip-loaded slot structure, the doped layers are identical to the slot width and thus $w_{\mathrm{Contact}} = w_{\mathrm{slot}} = 160$ nm. As a consequence the achievable phase-shift of the strip-loaded slot structure is about 13 times more efficien when the strip structure for the same applied voltage. Similarly, the achieveable phase-shift of the strip-loaded structure is about 6 times more efficien than the slot waveguide structure.

Finally, we should touch upon the art of poling the nonlinear polymer in the slot. Thanks to the fact that modulators come with metallic CPWs the active molecules of the nonlinear material can be aligned during fabrication by applying a poling voltage (green arrows) across the GSG electrodes. This way they are poled along the same direction. In operation, when an RF signal on the S-electrode is applied (red arrows), it will cause a positive phase shift in one arm and a negative phase shift in the other

one, which is exactly what is needed for to operate the MZI in push–pull operation mode.

C. Bandwidth Considerations

One of the most important characteristics of a modulator is its bandwidth which determines its modulation speed. For the strip-loaded slot waveguide shown in Fig. 1(c) switching can be performed with devices having a length of only 0.5 mm [48]. For such a length, the main bandwidth limitation derives from the *RC*-time constant, where C is the capacitance of the active region (slot), and R is the resistance of the strip-load. The next important limiting factor is the high attenuation of the radio frequency (RF) wave propagating on the travelling wave electrodes, which can be as high as 5 to 10 dB/mm at 100 GHz, see Table I and [32]. For longer devices and sufficientl low RF losses, also the walk-off between the optical and the electrical signal might become relevant [11], [32]. With these considerations in mind, we now discuss the bandwidth limitations in more detail. The discussion will be somewhat simplistic but useful to get an intuitive understanding. A proper design would require sophisticated modeling and intricate *RC*-circuit discussions [32], [49].

Electrical RC-limitations: In the strip-loaded MZI device depicted in Fig. 4, the voltage across the silicon rails should be at best the same as the voltage across the metal electrodes for any modulating frequency f. This requires charging of two slot capacitances C through the strip-load resistance R as depicted in the equivalent circuit in Fig. 5(a). The corresponding 3 dB bandwidth reads [11]

$$f_{3\mathrm{dB}} = \frac{1}{4\pi RC} \tag{5}$$

where the capacity of a single slot is C and the capacity for the two slots in an MZI is included by a factor 2 C. In order to increase the bandwidth, one either needs to decrease the capacity or decrease the sheet resistivity of the strip load. The capacity could be decreased by increasing the slot width—this however would be at the expense of increasing the operation voltage. The resistivity in the strip-load can be decreased by increasing the doping. This works well indeed and is frequently done. However, it comes at the price of higher optical losses due to the doped layers.

Recently, the resistivity was reduced and the bandwidth increased by applying a gate voltage that created a highly conductive electron accumulation layer at the silicon/silica–insulator interface [16], [48]. The scheme is shown in Fig. 5(a) and plots of frequency responses are shown in Fig. 5(b) and (c). The scheme works as follows. To generate a thin and highly conductive carrier accumulation layer, a voltage is applied between the strip loads and the bottom silicon substrate which acts as a gate. A thin carrier accumulation builds up at the interface between the silicon strip-load and the SiO_2 layer. We have plotted the frequency response of a 500 μm long phase-modulator section in Fig. 5(b). A 3 dB frequency response beyond 100 GHz can be seen. The data are normalized to a 10 dBm launch power (1 V amplitude at 50 Ω characteristic impedance). Fig. 5(c) shows that the frequency response increases when applying different

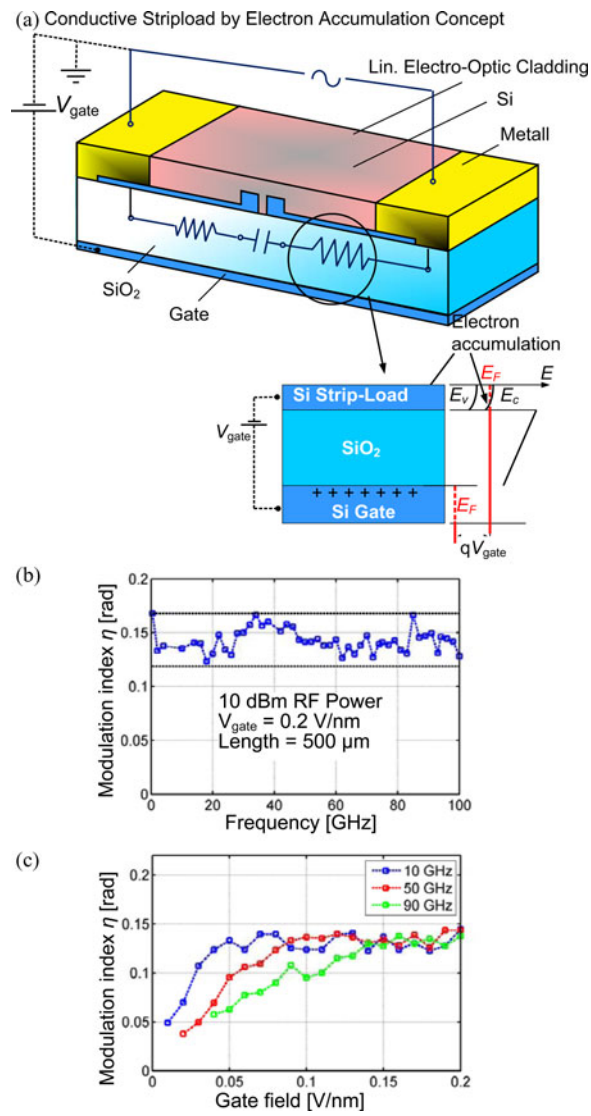

Fig. 5. Concept of an electron accumulation layer for increasing the stripload conductivity together with experimental results. (a) SOH-modulator showing a silicon slot waveguide connected to the metal electrodes by thin silicon strip-loads. In this concept the weakly doped silicon substrate acts as a gate electrode. When a positive gate voltage V_{gate} is applied across the 2-μm-thick SiO_2 substrate, a highly conductive electron accumulation layer forms in the strip-loads due to bending of the energy bands in the strip loads [16]. The thickness of the strip loads is 60 nm (not drawn to scale). $E_{F,C,V}$ are Fermi energy, conduction, and valence band energy, respectively; q is the elementary charge. The figur also shows the equivalent *RC* circuit for a short modulator section (slot capacitance C, strip-load resistance R). (b) Phase modulation index η versus frequency for a gate fiel of 0.2 V/nm. (c) Phase modulation index η versus gate fiel for selected modulation frequencies. The bottom two figur are taken from [48], where it is further shown how the gate voltage can be decreased.

gate fields Our measurements also indicate that for thin layers and a given sheet conductivity, one obtains lower losses with the accumulation layer technique rather than by doping. A thorough discussion of the effect is given in [31].

Limitations due to walk-off and microwave attenuation: Depending on device length and modulation frequency, one categorizes modulators into either "lumped" or "traveling wave (TW)" types. In the firs case, the device is much shorter than

the RF wavelength. In the second case, the modulator can in principle be arbitrarily long. However, spatial walk-off between electrical wave and optical signal as well as the RF attenuation impair the bandwidth. We now discuss these problems in more details.

The total phase change induced by an RF signal oscillating at the frequency f and propagating along a phase shifter of length L is given by [50]

$$\Delta\varphi(f,t) = \Delta\varphi_0 \cdot \frac{1}{L}\int_0^l e^{-\alpha_{el} z/2} \cos\left(2\pi f\left(\frac{\tau_{vm}}{L} z - t\right)\right) dz \tag{6}$$

where t is the time, $\Delta\varphi_0$ is the phase-change due to the linear electro-optic effect from a dc fiel and α_{el} is the RF power loss constant and the accumulated group delay τ_{vm} is

$$\tau_{vm} = \left|\frac{L}{v_{g,el}} - \frac{L}{v_{g,\mathrm{opt}}}\right| \tag{7}$$

with the electrical group velocity $v_{g,el}$ and optical group velocity $v_{g,\mathrm{opt}}$. Equation (6) shows how an induced phase shift $\Delta\varphi_0$ decreases with frequency in the presence of a group velocity mismatch or due a lossy coplanar microwave transmission line. If attenuation is neglected, the 3 dB bandwidth limitation associated with (6) is [11]

$$f_{\text{walk-off},3\,\mathrm{dB}} \cong \frac{0.5}{L}\frac{1}{\tau_{vm}}. \tag{8}$$

This walk-off usually can be neglected for mm-sized devices. For example, for a device of 1 mm length a large group delay of up to 5 ps would still result in a 100 GHz bandwidth.

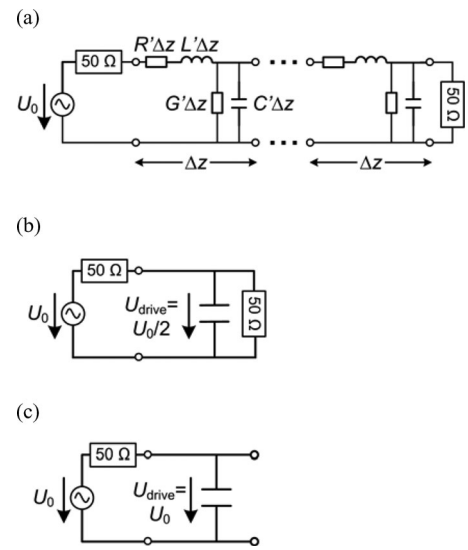

Fig. 6. Equivalent circuit models of various modulator types. (a) Traveling-wave modulator. The equivalent circuit of the modulator's transmission line is composed of a series of lumped elements of length Δz. The electrical drive signal is terminated by a 50 Ω load. R′, L′, G′, and C′ are series resistance, series inductance, shunt conductance, and shunt capacitance per unit length. U_0 is the open circuit peak voltage of the source. (b) Simplifie model of a terminated lumped modulator. The peak-drive voltage $U_0/2$ across the modulator input terminals is half the open-circuit source voltage U_0. The total RF power is dissipated by capacitive loading and by the 50 Ω termination. (c) Simplifie model of an unterminated lumped modulator. The on-chip drive voltage U_0 equals the open-circuit voltage of the source. Power dissipation inside the modulator is dominated by capacitive loading. Residual power is reflecte back to the source.

D. Energy Consumption

An advantage of the SOH modulator concept is its low energy consumption. The power consumption is low because of two effects [10], [11]. First, the modulating voltage drops across the narrow slot resulting in a high RF-fiel in the polymer infiltrate slot and second, because of organic materials with increasingly larger electro-optic coefficient [51]. To estimate the energy consumption, it is desirable to have closed-form expressions. We will firs derive approximate expressions for the energy consumption, and will then report on firs experiments demonstrating SOH modulators operating with as little as 60 fJ at 12.5 Gbit/s [52], [53]. The following discussion is mainly for illustrative purposes and requires more elaborate considerations for accurate results.

The power consumption can roughly be estimated with closed expressions for either of the two extreme cases of a lumped or a traveling wave modulator.

The traveling wave modulator, see Fig. 6(a), typically needs an electrical termination matched to the wave impedance in order to avoid reflection of RF waves that would interfere with the signal of the next bit. When a matched termination is used, the total power launched into the modulator is dissipated—in part by RF loss and capacitive loading, but eventually in the terminating resistor $R = 50\ \Omega$. The voltage amplitude across the modulator input terminal is $U_0/2$. For a dc-free rectangular drive voltage with a peak-to-peak open-circuit value $2U_0$, representing an alternating series of logical ones and logical zeros with a bitrate B_B, the energy consumption per bit can thus be approximated by $W_{\mathrm{bit}} = (U_0/2)^2/R/B_B$. TW modulators are energy-efficien when CPW losses are low and the optical and electrical CPW can propagate over long distances without walk off [54].

For a *lumped modulator,* the device is short and can be operated without terminating resistor. Many resonant modulator configuration in fact are lumped modulators that are usually operated without termination. Examples are slow-light structures [11], [55] or ring resonator structures [56], [57]. Short nonresonant modulators can also be operated without termination [53]. As an additional advantage of the unterminated lumped modulator, the in-device modulation voltage (the voltage made available at the electrodes of the device) is about U_0, i.e., it nearly doubles as explained in Fig. 6(c) as compared to the terminated case, Fig. 6(b). The energy consumption of the modulator is then dominated by the capacitive load of the slot waveguide. For the lumped device, we estimate the power dissipation associated with charging and decharging the total modulator capacitance $C_{\mathrm{MZM}} = 2\,C_{\mathrm{PM}}$ as seen by the CPW to be $W_{\mathrm{bit}} = C_{\mathrm{MZM}} \times U_{\mathrm{drive}}^2/4$, where C_{MZM} is the capacitance of the MZM comprising two PM and C_{PM} is the respective capacitance of one PM. This again assumes equal probabilities of logical ones and zeros, and it takes into account that only transitions consume energy [58].

As an illustrative example, we recently characterized a 10 Gbit/s on-off keying SOH-Modulator of 1.5 mm length with an 80 nm wide slot [52]. The modulator can be operated in two ways.

1) First, we operate the device with a 50 Ω termination and use a peak-to-peak drive voltage U_{drive} of 800 $\mathrm{mV_{pp}}$ (i.e., an amplitude of 400 mV_p). V_π – the voltage needed to switch an MZI modulator from minimum to maximum transmission was found to be 2.5 V_{pp} for high data rates. However, also smaller voltages suffic to get a clear and open eye. In our experiment the energy per bit thus was only 320 fJ when driving the modulator with 800 m V_{pp}.
2) Since the device is short and when limiting the bit-rate to a slower 10 Gbit/s, then operation without a termination is possible. At this data rate the modulator acts as a lumped device. The capacitance of the MZI modulator was found to be $C_{\mathrm{MZM}} = 2\ C_{\mathrm{PM}} = 378$ fF, which resulted in an energy consumption of 60 fJ/bit. Currents f owing due to bias and gate voltages were measured to be below 2 nA and below 100 fA, respectively, contributing a negligible energy consumption of less than 3 aJ/bit.

E. High-Data Rate Modulation Experiments

In this section, we demonstrate MZ and IQ modulators that generate advanced modulation formats at speeds up to 112 Gbit/s. The modulators exemplarily show that integrated circuits comprising fairly complex active and passive elements can be fabricated using the SOH platform. An in-depth description of both the structure and the experiment can be found in [47].

We implemented MZ and IQ-modulator configuration depicted in Fig. 3. For the fabrication, the silicon photonics platforms of IMEC and CEA-Leti were used to implement the structure of Fig. 7, where processes were optimized to allow a mass fabrication of the strip-loaded slot waveguide structure of Fig. 1(c). We use SOI wafers, which have a 220-nm high waveguide (WG) layer on a buried oxide (BOX) of 2 μm height. By employing 193 nm DUV lithography slot, WGs are patterned and subsequently etched into the WG layer ($w_{\mathrm{Slot}} = 140$ nm, $w_{\mathrm{Rail}} = 220$ nm, $h_{\mathrm{Rail}} = 220$ nm). Dry etching of 70 nm of Si is employed to make standard grating couplers [59] and rib WGs for low loss access waveguides [60]. Ion implantations are used to provide n-doped silicon strip-loads ($h_{\mathrm{Stripload}} = 50$ nm). A silicide f lm (on top of the highly doped silicon with nominally 1×10^{20} cm^{-3}) is created to guarantee a good electrical contact with the metallization. Different metallizations have been used for f rst experiments, gold or aluminium electrodes were deposited directly on the silicide striploads. For a more CMOS-compatible back-end stack, IMEC applied an oxide dielectic cover, and tungsten-fille vias then provided an electrical contact between the slot rails (guiding the optical field and the RF transmission line (guiding the electrical modulating wave) made of copper damascene electrodes. The slot is exposed using a selective dry+wet etch on the back-end. It is then functionalized with a commercially available electro-optic polymer (named M3 by the supplier GigOptix, Inc., [61], used in Telecordia certifie polymer modulators of the same manufacturer). It contains chromophores which are aligned in a poling procedure [62] inside the slot WG by applying a dc voltage at an elevated temperature to create the $\chi^{(2)}$ nonlinearity [18].

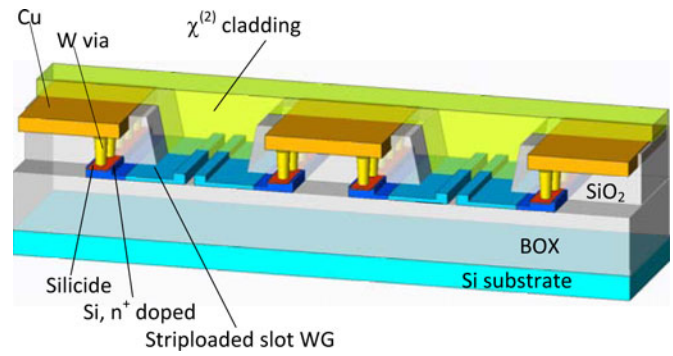

Fig. 7. Cross section through the phase-shifters of a strip-loaded slot phase-shifter section of an MZI structure as implemented in [47].

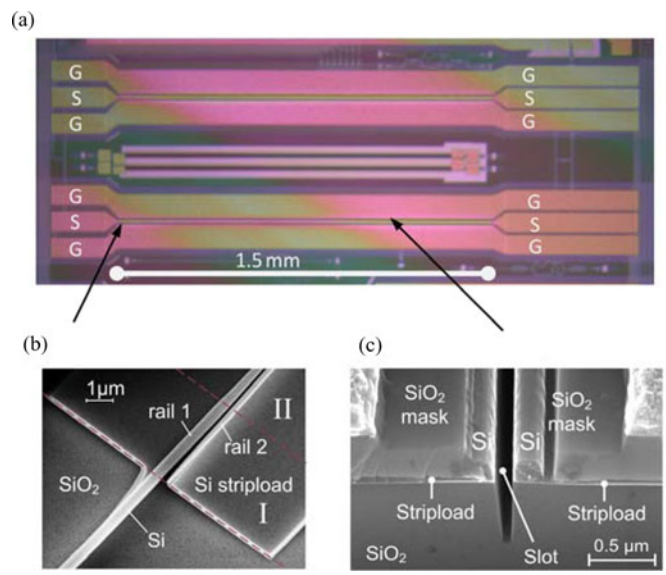

Fig. 8. Microscope Image of an SOH IQ-Modulator. (a) Two rows with MZ modulators and coplanar GSG waveguides are visible. (b) SOH strip-to-slot converter. (c) SEM image showing detail of the strip-loaded slot structure. The photos are taken from experiments described in [47], [28] and [16] respectively.

The MZ modulators consist of multimode interferometer couplers and the two phase modulator sections as schematically drawn in Fig. 3(a). The IQ-modulators consist of four phase modulator sections as depicted in Fig. 3(b). A photograph of a fabricated device is shown in Fig. 8. The strip-to-slot WG transitions are converters as outlined in Fig. 2 and discussed in [28] are shown in Fig. 8(b). Finally, we show an SEM image with the details of the strip-loaded slot structure in Fig. 8(c).

The experimental results below were achieved with a single polarization signal around 1540 nm. Data generation and reception experiments were performed in a standard test setup, as described in [47], using a PRBS of length 2^{11}–1. A software define transmitter was used to generate the electrical signals [38]. An advantage of this transmitter is that a preemphesis can be applied to the electrical signals for the generation of multilevel signals.

In Fig. 9, we show results obtained with SOH MZI modulators [63]. The plots in the upper row represent the constellation

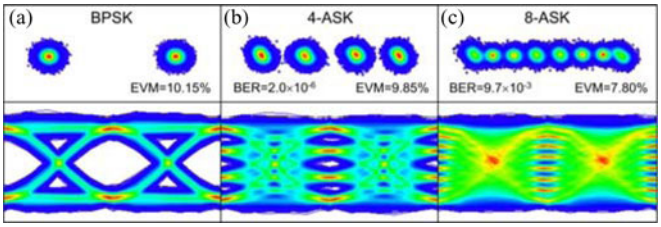

Fig. 9. SOH MZM constellation and eye diagrams for 28 GBd single polarization BPSK, 4-ASK and 8-ASK. (a) BPSK constellation and eye diagram with an EVM of 10.15% and a bit-error ratio below the detection limit of our setup. (b) 4-ASK constellation and eye diagram with EVM of 9.85% and a BER of 2×10^{-6}. (c) 8-ASK symbols with EVM of 7.80% and a BER of 9.7×10^{-3}. The bit rate of the 8-ASK signal is 84 Gbit/s [63].

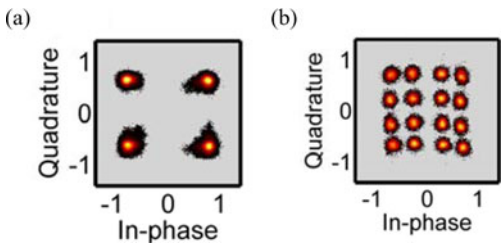

Fig. 10. SOH IQ modulator constellation diagrams for (a) 28 Gbd single polarization QPSK at 56 Gbit/s and (b) a 28 Gbd single polarization 16-QAM signal with a total of 112 Gbit/s [47].

diagrams obtained for BPSK, 4-ASK and 8-ASK signals at a symbol rate of 28 GBd. Bit-error ratio (BER) and error-vector magnitude (EVM) measurements [64] indicate that error-free operation is possible. All results prove a BER below the soft decision forward error correction limit. The plot in Fig. 9(c) shows an 8-ASK modulation format at 84 Gbit/s. The sampling scope traces at the bottom illustrate transitions between the various ASK levels. Even for the 8-ASK signal, one still can clearly see the eight levels at the center of the plot that correspond to the symbols in the constellation diagram above.

Results of the experimental tests performed with the SOH IQ-modulators are shown in Fig. 10, reported also in [47]. Fig. 10(a) displays the constellation diagram of a QPSK signal generated with an SOH modulator at a symbol rate of 28 GBd. This corresponds to a 56 Gbit/s signal. The symbols have clear and distinct shapes. The EVM was found to be 14.2% and bit-error ratios are well below the error detection limit of our setup. The constellation diagram in Fig. 10(b) shows how a 16-QAM signal can be generated with pre-emphasis at 28 GBd which corresponds to 112 Gbit/s. The symbols are round and distinct indicating a good signal quality. Measurements confir that we are below the hard-decision FEC limit with a BER of 1.2×10^{-3}. The EVM is 10.3% without equalization at the receiver,

IV. Silicon Phase-Shifters by Means of Liquid Crystals

Phase-shifters are also important building blocks in filter and other, especially interferometric configurations They should offer lowest power consumption but do not necessarily require fast operation. So far silicon photonic phase shifters are mainly based on the thermo-optic effect, where resistive heaters are co-integrated with SOI waveguides, and the large thermo-optic

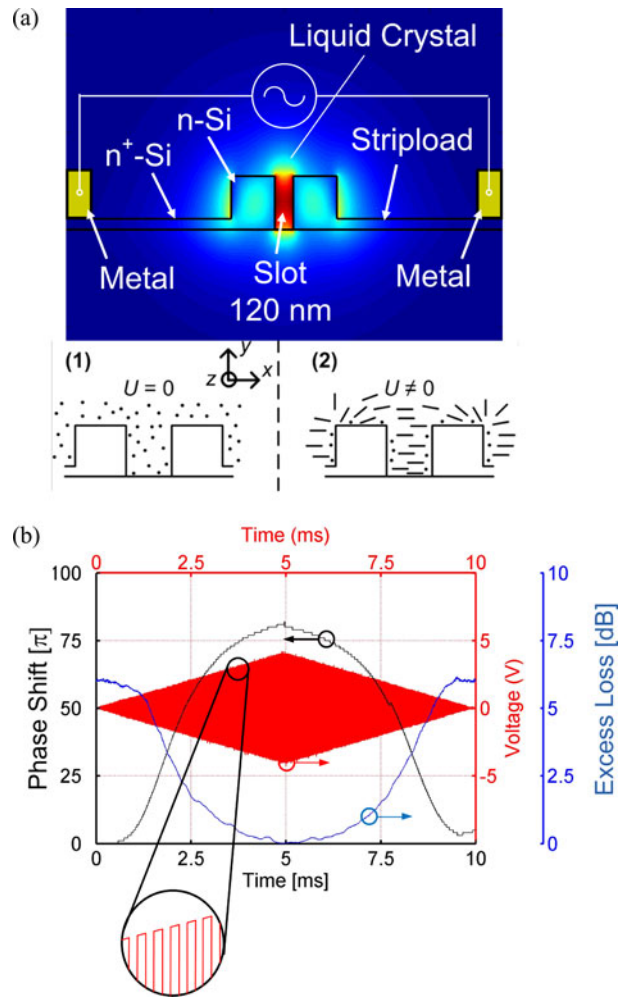

Fig. 11. (a) Configuratio of a silicon-organic hybrid (SOH) liquid crystal (LC) phase shifter. The bottom inset visualizes how LC aligns in the presence of an electric field If no external voltage is applied to the slot waveguide ($U = 0$), the LC molecules align parallel to the waveguide axis (1); for nonzero voltages $U \neq 0$, the LC will partly realign along the x-direction [20]. (b) Phase shift, applied voltage and excess optical loss versus time. The envelope of a 100 kHz square wave is modulated with a triangular function having frequency 100 Hz. The maximum electrical amplitude is 4 V. The maximum phase shift achieved is about 80 π. The device length is 1.7 mm [67].

coefficien of silicon is exploited to induce a phase shift by locally increasing the temperature [65].

By using the SOH platform in combination with a liquid crystal (LC) it is possible to achieve phase-shifting with extremely low power consumption [20], [25], [66]. In this section we report on a phase shifter with a record-small voltage-length product of $V_\pi L = 0.06$ V·mm [67]. This is obtained by combining liquid crystals with slot-waveguides built on the SOH platform [20].

Liquid-crystals are highly birefringent materials, which can reorient under the influenc of an electric field This makes them ideal candidates for electro-optic applications. Both the strip waveguide structure of Fig. 1(a) [25] as well the strip-loaded structure of Fig. 1(c) [20], [67] have been successfully used to demonstrate efficien phase-shifting. Yet, the strip-loaded slot configuratio is of particular interest because it allows applying a large electric fiel with small voltages in a purely capacitive input impedance configuration We therefore may expect lowest power consumption. [67]

Fig. 11(a) depicts the strip-loaded slot waveguide used in the experiment in a slightly different context as in Fig. 1(c). The external voltage is applied to the metallic electrodes located at a sufficien distance from the optical slot waveguide. The applied voltage drops entirely across the 120 nm wide slot, creating a strong electric fiel which can reorient the director of the liquid crystal deposited in the slot. The resistive silicon strips together with the capacitive slot act as an *RC*-circuit, whose time constant is negligible for the frequencies involved because of the slight doping of the silicon strips [16]. The phase shifter region is 1.7 mm long and has been fabricated in the silicon fab of CEA-Leti, see [16] for a detailed description. As a liquid crystal we used the commercially available E7 mixture, which is commonly used in liquid crystal displays.

In order to prevent ion migration in the liquid crystal, we applied a 100 kHz electrical square wave, as common in LC technology. The liquid crystal orientation, and therefore the optical phase shift, can then be tuned by varying the amplitude of the square wave. An example is depicted in Fig. 10(b), where the envelope of the 100 kHz square signal is modulated with a 100 Hz triangular wave having 4 V amplitude. The maximum phase shift achieved in the 1.7 mm long device is as high as 80 π (251 rad); see Fig. 10(b). Additionally, we observed a voltage-dependent insertion loss [see the blue curve in Fig. 10(b)], which is attributed to the light scattering occurring at the liquid crystal domain boundaries [68], [69]. The maximum slope of the phase-shift response corresponds to a voltage-length product of $V_\pi L = 0.06$ Vmm, which is, to the best of our knowledge, the smallest value ever reported so far in a silicon-based device.

The energy needed for varying the voltage from 0 to 4 V is less than 1 pJ. This low energy is due to the small capacitance in the order of 0.1 pF. Repeatedly varying the voltage at a frequency of 100 kHz would therefore lead to sub-μW power consumption. Some power is also dissipated by the parallel resistance of the device across the slot. This resistance is 20 GΩ, so that this power contribution is in the nW range only. Because of the high phase shifting efficien y, a device length of 100 μm is sufficien for most applications. In this case a π-shift could be obtained with a voltage swing smaller than 1 V, and with voltage-dependent losses below 0.3 dB. The power consumption would then decrease by another factor 16 because of the lower voltage.

V. Conclusion

The SOH platform addresses some of the main challenges of silicon photonics such as efficien nonlinear mixing and lasing but also enables highest speed Pockels effect modulation for optical communications and lowest voltage liquid-crystal phase-shifting. To this date, we have demonstrated high-speed modulators with a 3 dB bandwidth larger than 100 GHz, Mach–Zehnder modulators operating beyond 40 Gbit/s and IQ-modulators generating 16QAM at a data rate of 112 Gbit/s in one polarization with lowest power consumption. We have further discussed liquid–crystal phase-shifters and introduced them as a lowest-power alternative to the high-speed modulators. Liquid crystal PM are slow but operate at sub-μW powers.

References

[1] T. W. Baehr-Jones and M. J. Hochberg, "Polymer silicon hybrid systems: A platform for practical nonlinear optics†," *J. Phys. Chem. C*, vol. 112, pp. 8085–8090, Jan. 5, 2008.

[2] J. Leuthold, W. Freude, J. M. Brosi, R. Baets, P. Dumon, I. Biaggio, M. L. Scimeca, F. Diederich, B. Frank, and C. Koos, "Silicon organic hybrid technology—a platform for practical nonlinear optics," *Proc. IEEE*, vol. 97, no. 7, pp. 1304–1316, Jul. 2009.

[3] R. Won, "Integrating silicon photonics: Interview with Mario Paniccia," *Intel. Nat. Photon*, vol. 4, pp. 498–499, 2010. Available: http://dx.doi.org/10.1038/nphoton.2010.189.

[4] G. T. Reed, G. Mashanovich, F. Y. Gardes, and D. J. Thomson, "Silicon optical modulators," *Nat. Photon*, vol. 4, pp. 518–526, 2010.

[5] V. R. Almeida, Q. Xu, C. A. Barrios, and M. Lipson, "Guiding and confinin light in void nanostructure," *Opt. Lett.*, vol. 29, pp. 1209–1211, Jun. 1, 2004.

[6] M. Hochberg, T. Baehr-Jones, G. Wang, M. Shearn, K. Harvard, J. Luo, B. Chen, Z. Shi, R. Lawson, P. Sullivan, A. K. Y. Jen, L. Dalton, and A. Scherer, "Terahertz all-optical modulation in a silicon-polymer hybrid system," *Nat. Mater*, vol. 5, pp. 703–709, 2006.

[7] C. Koos, L. Jacome, C. Poulton, J. Leuthold, and W. Freude, "Nonlinear silicon-on-insulator waveguides for all-optical signal processing," *Opt. Exp.*, vol. 15, pp. 5976–5990, May 2007.

[8] C. Koos, P. Vorreau, T. Vallaitis, P. Dumon, W. Bogaerts, R. Baets, B. Esembeson, I. Biaggio, T. Michinobu, F. Diederich, W. Freude, and J. Leuthold, "All-optical high-speed signal processing with silicon-organic hybrid slot waveguides," *Nat. Photon*, vol. 3, pp. 216–219, 2009.

[9] T. Baehr-Jones, M. Hochberg, G. Wang, R. Lawson, Y. Liao, P. Sullivan, L. Dalton, A. Jen, and A. Scherer, "Optical modulation and detection in slotted Silicon waveguides," *Opt. Exp.*, vol. 13, pp. 5216–5226, 2005.

[10] M. Hochberg, T. Baehr-Jones, G. Wang, J. Huang, P. Sullivan, L. Dalton, and A. Scherer, "Towards a millivolt optical modulator with nano-slot waveguides," *Opt. Exp.*, vol. 15, pp. 8401–8410, Jun. 25, 2007.

[11] J.-M. Brosi, C. Koos, L. C. Andreani, M. Waldow, J. Leuthold, and W. Freude, "High-speed low-voltage electro-optic modulator with a polymer-infiltrate silicon photonic crystal waveguide," *Opt. Exp.*, vol. 16, pp. 4177–4191, Mar. 17, 2008.

[12] T. Baehr-Jones, B. Penkov, J. Huang, P. Sullivan, J. Davies, J. Takayesu, L. Jingdong, T.-D. Kim, L. Dalton, A. Jen, M. Hochberg, and A. Scherer, "Nonlinear polymer-clad silicon slot waveguide modulator with a half wave voltage of 0.25 V," *Appl. Phys. Lett.*, vol. 92, pp. 163303–163303-3, 2008.

[13] B. Esembeson, M. L. Scimeca, T. Michinobu, F. Diederich, and I. Biaggio, "A high-optical quality supramolecular assembly for third-order integrated nonlinear optics," *Adv. Mater.*, vol. 20, pp. 4584–4587, 2008.

[14] S.-S. Sun, L. R. Dalton, S.-S. Sun, and L. R. Dalton, *Introduction to Organic Electronic and Optoelectronic Materials and Devices (Optical Science and Engineering Series)*. Boca Raton, FL, USA: CRC Press., 2008.

[15] L. Dalton, P. Günter, M. Jazbinsek, O. P. Kwon, and P. A. Sullivan, *Organic Electro-Optics and Photonics*. Cambridge, U.K.: Cambridge Univ. Press, 2013.

[16] L. Alloatti, D. Korn, R. Palmer, D. Hillerkuss, J. Li, A. Barklund, R. Dinu, J. Wieland, M. Fournier, J. Fedeli, H. Yu, W. Bogaerts, P. Dumon, R. Baets, C. Koos, W. Freude, and J. Leuthold, "42.7 Gbit/s electro-optic modulator in silicon technology," *Opt. Exp.*, vol. 19, pp. 11841–11851, Jun. 6, 2011.

[17] L. Alloatti, D. Korn, C. Weimann, C. Koos, W. Freude, and J. Leuthold, "Second-order nonlinear silicon-organic hybrid waveguides," *Opt. Exp.*, vol. 20, pp. 20506–20515, Aug. 27, 2012.

[18] D. Korn, M. Lauermann, P. Appel, L. Alloatti, R. Palmer, W. Freude, J. Leuthold, and C. Koos, "First silicon-organic hybrid laser at telecommunication wavelengths," in *Proc. Lasers Electro-Optics Conf.*, 2012, pp. 1–2.

[19] M. Lauermann, D. Korn, P. Appel, L. Alloatti, W. Freude, J. Leuthold, and C. Koos, "Silicon-organic hybrid (SOH) lasers at telecommunication wavelengths," in *Advanced Photonics Congress*, OSA Technical Digest. (2012). [Online]. Optical Society of America, 2012, paper IM3A.3.

[20] J. Pfeifle L. Alloatti, W. Freude, J. Leuthold, and C. Koos, "Silicon-organic hybrid phase shifter based on a slot waveguide with a liquid-crystal cladding," *Opt. Exp.*, vol. 20, pp. 15359–15376, Jul. 2, 2012.

[21] T. Alasaarela, D. Korn, L. Alloatti, A. Säynätjoki, A. Tervonen, R. Palmer, J. Leuthold, W. Freude, and S. Honkanen, "Reduced propagation loss in silicon strip and slot waveguides coated by atomic layer deposition," *Opt. Exp.*, vol. 19, pp. 11529–11538, Jun. 6, 2011.

[22] S. K. Selvaraja, W. Bogaerts, P. Absil, D. Van Thourhout, and R. Baets, "Record low-loss hybrid rib/wire waveguides for silicon photonic circuits," presented at the Proc. Group IV Photonics, 7th Int. Conf., New York, NY, USA, 2010.

[23] J. F. Bauters, M. J. R. Heck, D. D. John, J. S. Barton, C. M. Bruinink, A. Leinse, R. G. Heideman, D. J. Blumenthal, and J. E. Bowers, "Planar waveguides with less than 0.1 dB/m propagation loss fabricated with wafer bonding," *Opt. Exp.*, vol. 19, pp. 24090–24101, 2011.

[24] B. Block, S. Liff, M. Kobrinsky, M. Reshotko, R. Tseng, I. Ban, and P. Chang, "A low power electro-optic polymer clad Mach-Zehnder modulator for high speed optical interconnects," *Proc. SPIE Silicon Photonics VIII, 86290Z*, vol. 8629, Mar. 14, 2013, doi:10.1117/12.2004489.

[25] W. De Cort, J. Beeckman, T. Claes, K. Neyts, and R. Baets, "Wide tuning of silicon-on-insulator ring resonators with a liquid crystal cladding," *Opt. Lett.*, vol. 36, pp. 3876–3878, Oct. 1, 2011.

[26] T. Vallaitis, S. Bogatscher, L. Alloatti, P. Dumon, R. Baets, M. L. Scimeca, I. Biaggio, F. Diederich, C. Koos, W. Freude, and J. Leuthold, "Optical properties of highly nonlinear silicon-organic hybrid (SOH) waveguide geometries," *Opt. Exp.*, vol. 17, pp. 17357–17368, Sep. 28, 2009.

[27] C. G. Poulton, C. Koos, M. Fujii, A. Pfrang, T. Schimmel, J. Leuthold, and W. Freude, "Radiation modes and roughness loss in high index-contrast waveguides," *IEEE J. Selected Topics Quantum Electron.*, vol. 12, no. 6, pp. 1306–1321, Nov./Dec. 2006.

[28] R. Palmer, L. Alloatti, D. Korn, W. Heni, P. C. Schindler, J. Bolten, M. Karl, M. Waldow, T. Wahlbrink, W. Freude, C. Koos, and J. Leuthold, "Low-Loss silicon strip-to-slot mode converters," *IEEE J. Photonics*, vol. 5, no. 1, pp. 2200409–2200409, Feb. 2013.

[29] C. Koos, L. Jacome, C. Poulton, J. Leuthold, and W. Freude, "Nonlinear silicon-on-insulator waveguides for all-optical signal processing," *Opt. Exp.*, vol. 15, pp. 5976–5990, May 14, 2007.

[30] R. Sun, P. Dong, N.-n. Feng, C.-y. Hong, J. Michel, M. Lipson, and L. Kimerling, "Horizontal single and multiple slot waveguides: Optical transmission at $\lambda = 1550$ nm," *Opt. Express*, vol. 15, pp. 17967–17972, 2007.

[31] L. Alloatti, M. Lauermann, C. Sürgers, C. Koos, W. Freude, and J. Leuthold, "Optical absorption in silicon layers in the presence of charge inversion/accumulation or ion implantation," *Appl. Phys. Lett.*, vol. 103, 051104, 2013.

[32] J. Witzens, T. Baehr-Jones, and M. Hochberg, "Design of transmission line driven slot waveguide?, Mach-Zehnder interferometers?, and application to analog optical links," *Opt. Exp.*, vol. 18, pp. 16902–16928, Aug. 2, 2010.

[33] J. Leuthold, C. Koos, and W. Freude, "Nonlinear silicon photonics," *Nat. Photon.*, vol. 4, pp. 535–544, 2010.

[34] J. Blasco and C. A. Barrios, "Compact slot-waveguide/channel-waveguide mode-converter," in *Proc. Lasers Electro-Optics Eur., Conf.*, 2005, pp. 607–607.

[35] Z. Wang, N. Zhu, Y. Tang, L. Wosinski, D. Dai, and S. He, "Ultracompact low-loss coupler between strip and slot waveguides," *Opt. Lett.*, vol. 34, pp. 1498–1500, May 15, 2009.

[36] A. D. Ellis, Z. Jian, and D. Cotter, "Approaching the non-linear shannon limit," *J. Lightw. Technol.*, vol. 28, pp. 423–433, 2010.

[37] R.-J. Essiambre, G. Kramer, P. J. Winzer, G. J. Foschini, and B. Goebel, "Capacity limits of optical fibe networks," *J. Lightw. Technol.*, vol. 28, pp. 662–701, Feb. 15, 2010.

[38] R. Schmogrow, D. Hillerkuss, M. Dreschmann, M. Huebner, M. Winter, J. Meyer, B. Nebendahl, C. Koos, J. Becker, W. Freude, and J. Leuthold, "Real-Time software-define multiformat transmitter generating 64QAM at 28 GBd," *IEEE Photonics Technol. Lett.*, vol. 22, no. 21, pp. 1601–1603, Nov. 2010.

[39] W. M. Green, M. J. Rooks, L. Sekaric, and Y. A. Vlasov, "Ultra-compact, low RF power, 10 Gb/s siliconMach-Zehnder modulator," *Opt. Exp.*, vol. 15, pp. 17106–17113, Dec. 10, 2007.

[40] L. Liao, A. Liu, J. Basak, H. Nguyen, M. Paniccia, D. Rubin, Y. Chetrit, R. Cohen, and N. Izhaky, "40 Gbit/s silicon optical modulator for high-speed applications," *Electron. Lett.*, vol. 43, no. 22, pp. 1196–1197, Oct. 2007.

[41] R. A. Soref and B. R. Bennett, "Electrooptical effects in silicon," *IEEE J. Quantum Electron.*, vol. 23, no. 1, pp. 123–129, Jan. 1987.

[42] P. Dong, C. Xie, L. Chen, L. L. Buhl, and Y.-K. Chen, "112-Gb/s monolithic PDM-QPSK modulator in silicon," *Opt. Exp.*, vol. 20, pp. B624–B629, Dec. 10, 2012.

[43] P. Dong, X. Liu, C. Sethumadhavan, L. L. Buhl, R. Aroca, Y. Baeyens, and Y.-K. Chen, "224-Gb/s PDM-16-QAM modulator and receiver based on silicon photonic integrated circuits," in *Proc. Opt. Fiber Commun. Conf./Nat. Fiber Opt. Eng. Conf. 2013, OSA Technical Digest*, paper PDP5C.6.

[44] D. J. Thomson, F. Y. Gardes, J. M. Fedeli, S. Zlatanovic, H. Youfang, B. P. P. Kuo, E. Myslivets, N. Alic, S. Radic, G. Z. Mashanovich, and G. T. Reed, "50-Gb/s silicon optical modulator," *IEEE Photonics Technol. Lett.*, vol. 24, no. 4, pp. 234–236, Feb. 2012.

[45] R. S. Jacobsen, K. N. Andersen, P. I. Borel, J. Fage-Pedersen, L. H. Frandsen, O. Hansen, M. Kristensen, A. V. Lavrinenko, G. Moulin, H. Ou, C. Peucheret, B. Zsigri, and A. Bjarklev, "Strained silicon as a new electro-optic material," *Nature*, vol. 441, pp. 199–202, 2006.

[46] B. Chmielak, M. Waldow, C. Matheisen, C. Ripperda, J. Bolten, T. Wahlbrink, M. Nagel, F. Merget, and H. Kurz, "Pockels effect based fully integrated, strained silicon electro-optic modulator," *Opt. Exp.*, vol. 19, pp. 17212–17219, Aug. 29, 2011.

[47] D. Korn, R. Palmer, H. Yu, P. C. Schindler, L. Alloatti, M. Baier, R. Schmogrow, W. Bogaerts, S. K. Selvaraja, G. Lepage, M. Pantouvaki, J. M. D. Wouters, P. Verheyen, J. Van Campenhout, B. Chen, R. Baets, P. Absil, R. Dinu, C. Koos, W. Freude, and J. Leuthold, "Silicon-organic hybrid (SOH) IQ modulator using the linear electro-optic effect for transmitting 16QAM at 112 Gbit/s," *Opt. Express*, vol. 21, pp. 13219–13227, 2013.

[48] L. Alloatti, R. Palmer, S. Diebold, P. Pahl, B. Chen, R. Dinu, M. Fournier, J. Fedeli, T. Zwick, W. Freude, C. Koos, and J. Leuthold, "100 GHz silicon-organic hybrid modulator," to be published.

[49] H. Yu, M. Pantouvaki, J. Van Campenhout, D. Korn, K. Komorowska, P. Dumon, Y. Li, P. Verheyen, P. Absil, L. Alloatti, D. Hillerkuss, J. Leuthold, R. Baets, and W. Bogaerts, "Performance tradeoff between lateral and interdigitated doping patterns for high speed carrier-depletion based silicon modulators," *Opt. Exp.*, vol. 20, pp. 12926–12938, Jun. 4, 2012.

[50] J.-M. Liu, *Photonic Devices*. New York, NY, USA: Cambridge Univ. Press, 2005.

[51] S. J. Benight, L. E. Johnson, R. Barnes, B. C. Olbricht, D. H. Bale, P. J. Reid, B. E. Eichinger, L. R. Dalton, P. A. Sullivan, and B. H. Robinson, "Reduced dimensionality in organic electro-optic materials: theory and define order," *J. Phys. Chem. B*, vol. 114, pp. 11949–11956, Sep. 23, 2010.

[52] R. Palmer, L. Alloatti, D. Korn, P. C. Schindler, M. Baier, J. Bolten, T. Wahlbrink, M. Waldow, R. Dinu, W. Freude, C. Koos, and J. Leuthold, "Low power mach-zehnder modulator in silicon-organic hybrid technology," *IEEE Photonics Technol. Lett.*, vol. 25, no. 13, pp. 1226–1229, Jul. 2013.

[53] R. Palmer, S. Koeber, W. Heni, D. L. Elder, D. Korn, H. Yu, L. Alloatti, S. Koenig, P. C. Schindler, W. Bogaerts, M. Pantouvaki, G. Lepege, P. Verheyen, J. Van Campenhout, P. Absil, R. Baets, L. R. Dalton, W. Freude, J. Leuthold, and C. Koos, "High-speed silicon-organic hybrid (SOH) modulator with 1.6 fJ/bit and 180 pm/V in-device Nonlinearity," in *Proc. Eur. Conf. Opt. Commun. (ECOC)*, paper We.3.B.3, Sep. 2013.

[54] T. Baehr-Jones, R. Ding, Y. Liu, A. Ayazi, T. Pinguet, N. C. Harris, M. Streshinsky, P. Lee, Y. Zhang, A. E.-J. Lim, T.-Y. Liow, S. H.-G. Teo, G.-Q. Lo, and M. Hochberg, "Ultralow drive voltage silicon traveling-wave modulator," *Opt. Exp.*, vol. 20, pp. 12014–12020, May 21, 2012.

[55] J. H. Wülbern, A. Petrov, and M. Eich, "Electro-optical modulator in a polymerinfiltrate silicon slotted photonic crystal waveguide heterostructure resonator," *Opt. Exp.*, vol. 17, pp. 304–313, Jan. 5, 2009.

[56] L. Chen, K. Preston, S. Manipatruni, and M. Lipson, "Integrated GHz silicon photonic interconnect with micrometer-scale modulators and detectors," *Opt. Exp.*, vol. 17, pp. 15248–15256, Aug. 17, 2009.

[57] J. C. Rosenberg, W. M. Green, S. Assefa, T. Barwicz, M. Yang, S. M. Shank, and Y. A. Vlasov, "Low-power 30 Gbps silicon microring modulator," in *Proc. CLEO:2011—Laser Appl. Photon. Appl., OSA Tech. Digest*, paper PDPB9.

[58] D. A. B. Miller, "Energy consumption in optical modulators for interconnects," *Opt. Exp.*, vol. 20, pp. A293–A308, Mar. 12, 2012.

[59] F. Van Laere, T. Claes, J. Schrauwen, S. Scheerlinck, W. Bogaerts, D. Taillaert, L. O'Faolain, D. Van Thourhout, and R. Baets, "Compact focusing grating couplers for silicon-on-insulator integrated circuits," *IEEE Photonics Technol. Lett.*, vol. 19, no. 23, pp. 1919–1921, Dec. 2007.

[60] W. Bogaerts and S. K. Selvaraja, "Compact single-mode silicon hybrid Rib/Strip waveguide with adiabatic bends," *IEEE J. Photonics*, vol. 3, no. 3, pp. 422–432, Jun. 2011.

[61] H. Chen, B. Chen, D. Huang, D. Jin, J. D. Luo, A. K. Y. Jen, and R. Dinu, "Broadband electro-optic polymer modulators with high electro-optic activity and low poling induced optical loss," *Appl. Phys. Lett.*, vol. 93, pp. 043507–043507-3, 2008.

[62] R. Blum, M. Sprave, J. Sablotny, and M. Eich, "High-electric-fiel poling of nonlinear optical polymers," *J. Opt. Soc. Amer. B*, vol. 15, pp. 318–328, Jan. 1, 1998.
[63] R. Palmer, L. Alloatti, D. Korn, P. C. Schindler, R. Schmogrow, W. Heni, S. Koenig, J. Bolten, T. Wahlbrink, M. Waldow, H. Yu, W. Bogaerts, P. Verheyen, G. Lepage, M. Pantouvaki, J. Van Campenhout, P. Absil, R. Dinu, W. Freude, C. Koos, and J. Leuthold, "Silicon-Organic hybrid MZI modulator generating OOK, BPSK and 8-ASK signals for up to 84 Gbit/s," *IEEE J. Photonics.*, vol. 5, no. 2, pp. 6600907–6600907, Apr. 2013.
[64] R. Schmogrow, B. Nebendahl, M. Winter, A. Josten, D. Hillerkuss, S. Koenig, J. Meyer, M. Dreschmann, M. Huebner, C. Koos, J. Becker, W. Freude, and J. Leuthold, "Error vector magnitude as a performance measure for advanced modulation formats," *IEEE Photon. Technol. Lett.*, vol. 24, pp. 2198–2198, Dec. 2012.
[65] M. S. Rasras, D. M. Gill, M. P. Earnshaw, C. R. Doerr, J. S. Weiner, C. A. Bolle, and Y.-K. Chen, "CMOS silicon receiver integrated with Ge detector and reconfigurabl optical filte ," *IEEE Photonics Technol. Lett.*, vol. 22, no. 2, pp. 112–114, Jan. 2010.
[66] B. Maune, R. Lawson, C. Gunn, A. Scherer, and L. Dalton, "Electrically tunable ring resonators incorporating nematic liquid crystals as cladding layers," *Appl. Phys. Lett.*, vol. 83, pp. 4689–4691, 2003.
[67] L. Alloatti, D. Korn, J. Pfeifle R. Palmer, S. Koeber, M. Baier, R. Schmogrow, S. Diebold, P. Pahl, T. Zwick, H. Yu, W. Bogaerts, R. Baets, M. Fournier, J. Fedeli, R. Dinu, C. Koos, W. Freude, and J. Leuthold, "Silicon-organic hybrid devices," in *Proc. SPIE*, 2013, p. 86290.
[68] Y.-H. Fan, Y.-H. Lin, H. Ren, S. Gauza, and S.-T. Wu, "Fast-response and scattering-free polymer network liquid crystals for infrared light modulators," *Appl. Phys. Lett.*, vol. 84, pp. 1233–1235, 2004.
[69] M. Kobayashi, H. Terui, M. Kawachi, and J. Noda, "2 × 2 optical waveguide matrix switch using nematic liquid crystal," *IEEE J. Quantum Electron.*, vol. 18, no. 10, pp. 1603–1610, Oct. 1982.

Juerg Leuthold (F'13) received the Ph.D. degree in physics from the Swiss Federal Institute of Technology (ETH), Zurich, Switzerland, in 1998. From 1999 to 2004, he was with Bell Labs, Lucent Technologies in Holmdel, NJ, USA, where he has been performing device and system research. From July 2004 to February 2013, he was a Full Professor at the Karlsruhe Institute of Technology, where he was the Head of the Institute of Photonics and Quantum Electronics, and the Head of the Helmoholtz Research Institute of Micro Structure Technology. Since March 2013, he has been a Full Professor at ETH Zurich. Dr. Leuthold is a Fellow of the Optical Society of America and a member of the Heidelberg Academy of Science.

Christian Koos received the Dr.-Ing. degree in electrical engineering from the University of Karlsruhe, Karlsruhe, Germany, in 2007. He has been a Professor at Institute of Photonics and Quantum Electronics, Karlsruhe Institute of Technology since 2010. From 2007 to 2008, he carried out Postdoctoral research at the Institute of Photonics and Quantum Electronics, University of Karlsruhe. From 2008 to 2010, he was with the Corporate Research and Technology department of Carl Zeiss AG, Germany.

Wolfgang Freude received the Dipl.-Ing. (M.S.E.E.) and the Dr.-Ing. (Ph.D.E.E.) degrees in electrical engineering from the University of Karlsruhe, Karlsruhe, Germany, in 1969 and 1975, respectively. He is a Professor at Karlsruhe Institute of Technology. Dr. Freude is currently a Subcommittee Chair for CLEO: 2013. Until 2010, he was the Vice Chair of the IEEE Germany Photonics Society.

Luca Alloatti was born in 1980 in Turin, Italy. He received the Graduation degree in physics (Hons.) at the University of Pisa, the "Diploma di Licenza" (Hons.) from the Scuola Normale Superiore, Pisa, Italy, and the Ph.D. degree from the Karlsruhe Institute of Technology (KIT), Karlsruhe, Germany, in 2004, 2006, and 2012, respectively. He is currently a Postdoctoral Researcher at the Institute for Photonics and Quantum Electronics at the KIT.

Robert Palmer received the Diploma degree in Physics (Hons.) from the Karlsruhe Institute of Technology (KIT), Germany, and is currently working toward the Ph.D. degree in electrical engineering. He is a Research Associate at Institute of Photonics and Quantum Electronics, KIT His research interests include Silicon Photonics and define by the BMBF project MISTRAL.

Dietmar Korn received the Diploma degree in physics from the University of Potsdam, Potsdam, Germany, and is currently working toward the Ph.D. degree in electrical engineering. He is a Research Associate at the Institute of Photonics and Quantum Electronics, Karlsruhe Institute of Technology, Karlsruhe, Germany, aff liated with Karlsruhe School of Optics and Photonics. His research interests include integrated optics and define by the EU project www.sofi-ict.e about the Silicon Organic hybrid Fabrication platform for Integrated circuits, which he manages.

Joerg Pfeifle received the Dipl.-Ing. degree in electrical engineering from the Karlsruhe Institute of Technology in 2010, where he is currently working towards the Ph.D. degree. His research interest includes design, fabrication and characterization of devices for integrated high-capacity and energy-efficien optical interconnects.

Matthias Lauermann received the Diploma degree in 2011 from the Department of Electrical Engineering and Information Technology, Karlsruhe Institute of Technology (KIT), Germany, where he is currently working toward the Ph.D. degree in the Group of Prof. Christian Koos. His research interest includes around the integration of hybrid silicon photonic systems.

Raluca Dinu received the B.Sc. degree in optics and the Ph.D. degree in physics from the University of Bucharest, Bucharest, Romania, in 2000, in ferroelectric thin film for random access memories. She also graduated from the Executive MBA AeA/Stanford Institute, Stanford, CA, USA, in 2007. In 2008, She joined GigOptix as the Vice President of Product Development after having served as the Vice President of the Electro-Optic Business Unit since 2007 for Lumera Corporation. She holds 15+ patents and successfully brought the polymer-based business TFPS technology to production.

Silvan Wehrli (S'07) was born in Zürich, Switzerland, in 1980. He received the M.Sc. degree in electrical engineering and information technology from the Swiss Institute of Technology of Zürich (ETHZ), Zuerich, Switzerland, in 2005, and the Ph.D. degree from the Electronics Laboratory, ETH Zuerich, Switzerland for his thesis "Integrated Active Pulsed Reflecto for an Indoor Positioning System." His work in GigOptix mainly focuses on chip design for multichannel optical transceivers for high data rates.

Mojca Jazbinsek received the Ph.D. degree in physics in 2001 from the University of Ljubljana. Following the graduation, she moved to ETH Zurich, Switzerland, where she was working as a Project Leader at the Nonlinear Optics Laboratory, Institute of Quantum Electronics. In 2010, she moved to the spin-off company of ETH, Rainbow Photonics AG, where she is currently working on applied research projects on organic nonlinear optical materials for electro-optics and THz-wave generation, as well as development of commercial THz sources.

Peter Günter studied at Swiss Federal Institute of Technology (ETH) and received the Master's degree (dipl. Phys. ETH) in 1971 and the Ph.D. degree in physics in 1976. He is currently an Emeritus Professor of physics at ETH. In 1982 he became Privatdozent (Senior Lecturer) and from 1986 to 2008, he was a Professor of experimental physics and the Head of the Nonlinear Optics Laboratory at ETH. His research interests include electro-optics, nonlinear optics, integrated optics, and optical microresonators, photorefractive phenomena in organic and inorganic materials, terahertz. Dr. Günter is and was a member of the editorial board of various journals and he is a Fellow of the Optical Society of America.

Michael Waldow received the Diploma degree in electrical engineering at the University of Karlsruhe, Karlsruhe, Germany, on design of high speed integrated 40 Gb/s modulators, in 2006, and the Ph.D. degree in photonics at Institute of Semiconductor Technology, RWTH Aachen, Aachen, Germany. After being with Bell-Labs, Crawford Hill for an internship he worked for f ve years as a Scientist at RWTH Aachen, Institute of Semiconductor Technology (2006–2011. Since 2011, he is leading the Nanophotonic Group at AMO, where he is responsible for several European and national projects in the f eld of nanophotonics. He has authored and coauthored several journal papers and conference proceedings.

Thorsten Wahlbrink received the Diploma degree and the Ph.D. degree in physics from the University of Osnabrück, Osnabrück, Germany (2001). He is a Senior Research Scientist at AMO GmbH, Aachen, Germany (2001-today). He conducted research on nanoscaled transistor devices and fabrication processes for integrated silicon photonic devices. Furthermore, he is primarily responsible for the e-beam lithography at AMO. He has worked in several national and European funded nanophotonic projects and successfully coordinated the FP6 project "Circles of Light." He is author or coauthor of several publication of advanced processing for integrated nanophotonic devices.

Jens Bolten received the Diploma degree in electrical engineering at RWTH Aachen, Aachen, Germany, in 2006, and the Ph.D. degree in 2012. Since 2006, he has been a Research Scientist at AMO GmbH, Aachen, Germany. His research interests include electron beam lithography as a prototyping technology for advanced and novel nanoelctronic and nanophotonic devices. He has authored and coauthored several journal papers and conference proceedings within the f elds of his research.

Heinrich Kurz received the diploma and Ph.D. degrees in physics from the University of Wien, Vienna, Austria, in 1968 and 1971, respectively. After spending time at the Philips-Research center in Hamburg and at Harvard University he became a Professor at RWTH in Aachen, Germany, in 1984. In 1990, he is a Full Professor at RWTH Aachen. Since 1993 and 1997, he is also heading the AMO GmbH and AMIC Center in Aachen.

Maryse Fournier received the Graduation degree from the Conservatoire National des Arts et Métiers, Grenoble, France, in 1993. In 2010, she joined Silicon Photonics' Group, CEA, Grenoble, France, in order to take in-charge of the ePIXfab activity on FP7-PHOTONFAB, followed by FP7-ESSenTIAL Support Action.

Jean-Marc Fedeli received the Diploma degree in electronics engineer from Grenoble Institute of Technology Grenoble, France, in 1978. Then he conducted researches at the CEA-LETI on various magnetic memories and magnetic components as a Project Leader, Group Leader, and Program Manager. Under a large partnership with universities and research laboratories, he works on various technological aspects on Photonics on CMOS. Under the European FP7, was program manager of the HELIOS project. He is currently managing the FP7 PLAT4M project on Silicon Photonics Platform and involved in a CELTIC project as well as industrial projects on Silicon Photonics.

Hui Yu received the Bachelor's degree in electrical engineering, and the Ph.D. degree in electrical engineering from Zhejiang University, Hangzhou, China, in 2003 and 2008. In 2009, he joined the Photonics Research Group, Ghent University, Ghent, Belgium as a Postdoctoral Researcher, where he worked on silicon electro-optic modulators until 2012. He is currently a Lecturer with the Department of Information science and electronic engineering, Zhejiang University, Hangzhou, China.

Wim Bogaerts (M'98) studied engineering at Ghent University, Gent, Belgium, where he subsequently received the Ph.D. degree and IMEC in 2004. He is a Professor in the Photonics Research Group, Ghent University He specialized in the modeling, design, and fabrication of nanophotonic components. As a Professor, he focuses research on design challenges in large-scale silicon photonics. Dr. Bogaerts is a member of the IEEE Photonics Society, the Optical Society of America (OSA) and SPIE.